PNCT N9410 90-069

Presented at the 11th annual
conference of the Canadian
Nuclear Society, Toronto, Ontario, Canada
June 3-6, 1990.

DEVELOPMENT OF AN ANALYTICAL METHOD TO EVALUATE THE INTEGRITY OF A CALANDRIA TUBE IN THE CASE OF PRESSURE TUBE RUPTURE

MAY, 1990

OARAI ENGINEERING CENTER
POWER REACTOR AND NUCLEAR FUEL DEVELOPMENT CORPORATION

DEVELOPMENT OF AN ANALYTICAL METHOD TO EVALUATE THE INTEGRITY OF A CALANDRIA TUBE IN THE CASE OF PRESSURE TUBE RUPTURE

Y. MORISHITA, I. MATSUSHITA, H. MOCHIZUKI AND Y. HAYAMIZU

O-arai Engineering Center
Power Reactor and Nuclear Fuel Development Corporation
4002 Narita, O-arai, Ibaraki-ken, 311-13, Japan

ABSTRACT

An analytical method which consists of two-dimensional thermal-hydraulic analysis and three-dimensional structural analysis has been proposed to evaluate the integrity of a calandria tube in the case of pressure tube rupture in a pressure tube type reactor. In order to validate the method, experiments were carried out with coaxially arranged double tubes simulating a pressure tube and a calandria tube. Experimental data were also compared with analytical results with the proposed method.

INTRODUCTION

The Advanced Thermal Reactor (ATR) being developed in Japan is a boiling-light-water-cooled heavy-water-moderated pressure-tube-type reactor. The core of ATR consists of an array of a vertical pressure tube surrounded with a coaxial calandria tube passing through a calandria vessel, as shown in Fig.1. The pressure tubes contain the fuel bundles. 7MPa boiling light-water as a coolant is circulated in the pressure tube. The calandria vessel is filled with a roughly 70 °C heavy-water moderator insulated from the high-temperature reactor coolant by a CO_2 gas filled annulus between the pressure tube and the calandria tube. In the case of pressure tube (PT) rupture in ATR, a calandria tube (CT) is expected to withstand failure of the PT and surve as a pressure boundary instead of the PT. The integrity of the CT is, therefore, of prime concern in safety assessment.

When a PT ruptures, the following are supposed; namely, the ruptured lips of the PT spread in a radial direction and collide with the CT surrounding the PT, the coolant in the PT is discharged into the annulus from an opening of the ruptured PT, and the pressure of the annulus rises because of the discharged coolant. At this time, the CT is also supposed to be subjected to some loads, which are mainly the impact loading caused by collision of the PT with the CT, the risen pressure and thermal stress caused by temperature rise of the CT.

The objectives of this study are to clarify the dominant load for the integrity of the CT and to develop the analytical model for predicting the dominant load and deformation of the CT. As a first step in the development of the analytical method, semi-scale experiments were carried out to clarify the behavior of the loads acting on the CT in the case of PT rupture and the dominant load to the CT. The analytical method which consists of a thermal-hydraulic analysis and a structural analysis is proposed to predict

the deformation behavior of the CT subjected to the impact loading regarded as the most serious load to the CT from experimental results. The applicability of the proposed method is also investigated through the experimental analyses. The analytical results are compared with experimental data.

EXPERIMENTS

Experiments were conducted to clarify the loading behavior to the CT and the dominant load for the integrity of the CT. The test section employed in the experiments consisted of coaxially arranged inner and outer tubes simulating a PT and a CT, respectively. They were positioned horizontally in the atmosphere as shown in Fig.2. The inner tube was made of carbon steel, and the outer tube, stainless steel or Zr-2 alloy. Outer diameter of the inner tube and inner diameter of the outer tube are the same sizes as those of a PT and a CT of an actual plant, and are 126.4mm and 158.4mm, respectively. A 36-rod fuel bundle simulator was provided in the inner tube to simulate the flow area inside the PT. In order to simulate the flow resistance of discharged coolant into the atmosphere, orifices were provided at both ends of the annulus. An axial notch, which was designed so that it might rupture at the pressure ranging from 5 to 7MPa, was machined on the outer surface of the inner tube. The coolant was circulated with a pump through the inner tube. The coolant was heated and pressurized by electric heaters until the tube ruptured.

The pressures in the inner tube and in the annulus between the tubes, the strains of the tubes and the temperature of the outer tube were measured at positions shown in Fig.3. Regarding pressure measurement, piezo-type pressure transducers of which the resonant frequencies are 50KHz were used. The time of initiation of the rupture and the extension speed of the crack were measured with crack gauges attached to the surface of the inner tube along the notch. Mean hoop strains of the outer tube at several axial positions including the starting point of the crack extension were also measured after the experiments. Data were sampled at intervals of 0.05 milliseconds. A summary of experimental conditions and results are shown in Table 1.

Experimental results showed that the impact loading, the maximum pressure rise in the annulus and the maximum thermal stress occured at about 1 millisecond, 0.5 seconds and 1 second, respectively (Fig.4). The maximum pressure rise in the annulus was nearly equal to the initial pressure of the coolant inside the inner tube under the condition of 10 °C in subcooling. The most serious loading to the outer tube was the impact loading according to the experimental results. Figure 5 shows the immediate histories of the pressure and the strains after the rupture. The pressure inside the inner tube decreased rapidly at 0.2 milliseconds below the saturated pressure level. This behavior suggests that the depressurization inside the inner tube was caused by increase in the volume inside the tube due to spread of tube wall and thermal non-equilibrium of the coolant. The overheated coolant inside the inner tube started to boil significantly at about 0.6 milliseconds, resulting in a 0.4 milliseconds delay of initiation of boiling. The wall of the inner tube was accelerated to spread by the pressure acting on it. The coolant was discharged from the spread opening, and it resulted in the rapid pressure rise on the inner surface of the outer tube at the front of the opening. The impact occured at about 1.2 milliseconds when the strain (PT-1) of a ruptured lip increased abruptly. Figure 6 shows the relation between the

pressure inside the inner tube integrated with time until occurrence of the collision and the strain energy calculated from the mean hoop strain of the outer tube. The integrated pressure is equivalent to the impulse applied on the inner tube. The strain energy increased with the impulse. Thus, the impact loading caused by the spread of the inner tube depends on the pressure acting on it.

ANALYSIS

As is obvious from the experimental results, the impact loading, which was the most serious load and occured very early(1-2 msec) after the rupture, depends on the pressure acting on the inner surface of the ruptured PT. The pressure in the ruptured PT, which decreased rapidly after the rupture, is affected by the thermal non-equilibrium of the coolant and deformation of the PT. It is, therefore, necessary that both the deformation behavior of the ruptured PT and the thermal-hydraulic behavior in the PT are considered in numerical analysis to evaluate the impact loading. The subject of this type of analysis is a fluid-structure interaction problem. Analytical codes such as PISCES[1] and AUTODYN[2], which are extensively applied to the fluid-structure interaction ploblem, cannot calculate the effect of thermal non-equilibrium. Therefore, we have been developing an analytical method capable of treating both the deformation of the PT and the thermal non-equilibrium of the coolant.

The analytical method proposed in this study consists of the thermal-hydraulic analysis[3] to predict the pressure transient inside the ruptured PT and the structural analysis to predict the strain generated in the CT by collision of the PT with the CT.

Thermal Hydraulic Analysis

Analytical Model. Thermal-hydraulic behavior of the coolant was treated by a two-dimensional six equation scheme based on the two-fluid model for two-phase mixture. The rapid depressurization under the thermal non-equilibrium condition is controlled by the superheat of the liquid phase of the two-phase mixture. Hence, a mass exchange rate between the liquid and steam phases was estimated using the non-equilibrium vapor production model. The mass exchange rate, Γ, is defined by the following equation;

$$\Gamma = J_e - J_c ,$$

where J_e stands for evaporation rate and J_c , condensation rate. Regarding J_e, the non-equilibrium vapor production model[4] expressed by the following equation was adopted:

$$J_e = \rho_l \left(\frac{18}{\pi}\right)\left(\frac{\theta}{r_b^2}\right)\left(\frac{\rho_l}{\rho_g}\right)\alpha_l \left\{\frac{C_l(T_l - T_s)}{L}\right\}^2 ,$$

where r_b is bubble radius; α_l, liquid thermal diffusivity; C_l, liquid specific heat; T_s, saturated temperature; and L, latent heat. On the other hand, in the rapid depressurization process within a few milliseconds, condensation usually plays rather an insignificant role on the mass exchange rate. Therefore, J_c was assumed to be zero.

The six equations representing mass, momentum and energy conservation for each phase were discretized using the forward-time and upwind differences. In this discretizing, a moving boundary method was adopted to treat the spread of the PT wall in a radial direction. In Fig.7, cell [1] indicates a typical discretized cell with a moving boundary which corresponds to the section of the PT wall. When the boundary with a cross section A moves at the velocity U_b, the volume of the cell [1], V^n at the time of t^n is enlarged at the next time step t^{n+1} to v^{n+1} given by

$$V^{n+1} = V^n + \Delta t\, U_b\, A\,,$$

through time-marching process of the numerical integration of the equations. In order to take into account the change in the opening area, moreover, the concept of transmission area was introduced on the basis of a porosity model. For the cell with the opened boundary, the transmission area, S^n was defined by

$$S^{n+1} = \alpha^{n+1} A\,,$$

where a transmission factor α is given by the ratio of the opening area, a and the cross sectional area. A as

$$\alpha^{n+1} = a / A\,.$$

With the use of this S^n, discharge flow volume, Q from the cell [1] to the adjacent cell [2] for Δt is obtained by

$$Q = S^{n+1} (U_f - U_b)\, \Delta t,$$

where U_f stands for fluid velocity.

Experimental Analysis. The analytical model discribed so for was validated through the analysis of the semi-scale experiments. The test section in the experiments was modeled by the mesh system illustrated in Fig. 8. On the assumption that the thermal-hydraulic behavior is axially symmetric in the test section, the inside of the inner tube and annulus space between tubes were divided equally into nine cells in the circumferential direction. The fuel bundle simulator was replaced by a column of which the sectional area is equivalent to that of the simulator.

Applicability to the rapid depressurization process has not been fully examined for the existing correlations of interfacial friction between water and steam. However, it was confirmed that calculational results were insensitive to the selection of the correlation. Consequently, we used so large interfacial friction coefficient that the liquid and steam could move at the same velocity. The information on the deformative motion of the inner tube is indispensable for calculating the thermal-hydraulic transient after the rupture. Thus, the deformative motion was determined with the code DYNA-3D[5] from pressure histories measured at an inner surface of the inner tube. Because the calculation by the code DYNA-3D could not reproduce the time of the collision of the inner tube with the outer tube, however, the time scale in the calculated results was modified by the ratio of the calculated and measured collision times before utilizing

them in the thermal-hydraulic calculation. Figure 9 illustrates the modified deformative motion after the rupture. The transmission factor α was also determined for each cell from the calculated deformative motion in accordance with the definition described above. Although small deformation was observed in the outer tube after the collision of both tubes, the effect of this deformation was not taken into account in the thermal-hydraulic analysis. Furthermore, heat transport across the walls of the inner and outer tubes was assumed to be negligible.

The calculational pressure transients in the inner tube and the annulus are compared with the experimental data in Fig.10. As for the inside pressure of the inner tube, the observed sudden decrease at about 0.2 milliseconds after the rupture is well reproduced with the calculation. This suggests that the adoption of the moving boundary method is essential in the analysis of the depressurization phenomena due to the rapid change in volume. The calculational annulus pressure increases rapidly at about 0.8 milliseconds after the rupture and reaches the maximum when the lip of the ruptured tube collides with the outer tube.

Structural Analysis

Analytical Model. A three-dimensional shell model was applied to the analysis of the structural behavior of the PT, especially in order to properly predict the rigidity effect where ruptured lips of the PT are restrained from freely deforming. Because this rigidity effect strongly depends upon the length of the crack on the PT, it is essential to treat appropriately the crack extension with definite speed. Hence, the following model was adopted; the ruptured lips are considered to tightly connect with each other initially by a superficial chain of springs whose elastic constants are equal to the value estimated from Young's modulus of the material of the PT, as illustrated in Fig.11. And the elastic constant of the spring at the position where the edge of crack reaches is set to zero by turns with extending the crack. The time when the elastic constant of the spring is set to zero, T_i, is given by

$$T_i = L_i / U_c, \quad (i=1,2,.....,n) ,$$

where, L_i is distance from the starting point of the crack to a point where the spring is provided, and U_c is the crack extension speed (see Fig.12).

Experimental Analysis. An experimental analysis was conducted for the experiment of test No.2 shown in Table.1 with the code DYNA-3D[5]. DYNA-3D is the code for three-dimensional impact stress analysis and can handle contacts of structural objects considering the slidings on surfaces of the contacts. A mesh system illustrated in Fig.11 was adopted to predict the strain generated in the outer tube. Deformation of both the inner tube and the outer tube in a radial direction was assumed to be symmetrical between the upper and lower halves. Deformation of both tubes in an axial direction was also assumed to be symmetrical between the right and left halves at the initial point of the crack. The inner tube and the outer tube of the model consist of 18 shell elements in a circumferential direction, respectively. The axial length of the model adopted in the analysis was selected as 400mm to allow for crack length until the collision occured. The crack extension speed was set to be equal to that which was measured in the experiment. In the analysis, the pressure histories measured in the

experiment were given on the inner surface of the inner tube divided into three equal parts, assuming that the pressure acting on the inner surface was uniform in each part.

The calculated mean hoop strain at the starting point of the crack extension and the local strains at measuring points are compared with experimental data, as shown in Fig.13. The three dimensional model predicts the mean hoop strain at the starting point of the crack extension within ±20% of error, and the histories of the local strains.

DISCUSSION

The calculation succeeds in reproducing overall profile of the experimental pressure transients, as shown in Fig.10; especially the calculated pressure increases without time lag after the experimental rapid depressurization at 0.2 milliseconds. Regarding the pressure charge after the rapid depressurization, on the other hand, the measured pressure in the inner tube remains at a lower level for a while and rises gradually while the calculated pressure starts to rise rather sooner. This difference obsereved in the pressure recovery phase is supposed to result from the neglect of delayed evaporation in the calculation. Regarding the pressure behavior in the annulus, the calculated pressure rises higher than the measured pressure at 0.8 milliseconds. The higher pressure rise in the analysis is supposed to be caused by stagnation of discharge flow due to the collision of the ruptured lips with the outer tube. The two-dimensional analysis overestimates the effect of obstructing; however, in the experiment, the coolant may be discharged into the annulus in an axial direction as well as radial direction so that the pressure rise at 0.8 milliseconds may be mitigated.

The capability of the three-dimensional model in the structural analysis was assessed by comparing the analysis by the two-dimensional model. The calculated pressure histories given as loading conditions on the inner surface of the inner tube were the same as those given in the three-dimensional analysis. As shown in Fig.13, the two-dimensional model predicts the mean hoop strain of the outer tube larger than the three-dimensional model, and does not simulate the histories of the local strains. The difference of both results is due to the difference of rigidity effect of the lips.

The thermal-hydraulic analysis and the structural analysis proposed in this study, are coupled in an analysis of the integrity of the CT in the case of the PT rupture. In the series of the analysis, the thermal-hydraulic analysis is executed by considering both movement of the boundaries and the transmission factors of the boundaries which are defined from calculating results of the structural analysis. In the structural analysis, the deformation of both tubes are calculated on the basis of loading conditions which are given by calculating results of the thermal-hydraulic analysis.

CONCLUSIONS

The followings are obtained from both semi-scale experiments simulating the PT rupture and the investigations of the analytical method.

(1) The impact loading, the pressure rise and the thermal stress, which act on the CT after the PT rupture, are individual regarding the occurrence time. The most serious load to the CT is the impact loading which occurs at about 1 millisecond after the rupture.

(2) Thermal-hydraulic behavior of the coolant after the rupture can be predicted by use of a combination of the vapor production model for the thermal non-equilibrium, the moving boundary for the spread of the ruptured lips, and the porosity model for the opening area change.

(3) Deformation behavior of the CT caused by the collision of the ruptured PT can be predicted by use of the three-dimensional shell model considering the crack extension speed after the rupture.

REFERENCES

(1) HANCOCK, S., "PISCES-2DELK Theoretical Manual", PISCES International bv, 1985.

(2) BIRNBAUM, N. K., COWLER, M. S., ITOH, M., KATAYAMA, M, and OBATA, H., "AUTODYN - an interactive non-linear dynamic analysis program for microcomputers through supercomputers", 9th Internat. Conf. on Structural Mechanics In Reactor Technology, Lansanne, Switzerland, 1987, August.

(3) MORISHITA, Y., MATSUSHITA, I., HAYAMIZU, Y. and KUDO, Y., "Analysis of Pressure Transient with Moving Boundary caused by Tube Rupture under thermal Non-equilibrium Conditions", 1st Internat. Conf. Supercomputing in Nuclear Applications, JAERI, Japan, 1990, March.

(4) RIVARD, W. C. and TRAVIS, J. R., "A Non-equilibrium vapor production model for critical flow", Nuclear Science and Engineering, Vol.74, pp 40-48, 1980.

(5) HALLQUIST, J. O., "DYNA 3D User's manual rev.4", Lawrence Livermore National Laboratory, 1988.

Table 1. Summary of test conditions and results

Test No.	Inner tube	Outer tube	Burst pressure (Mpa)	Fluid temperature (℃)	Void fraction (−)	Crack extension speed (m/s)	Mean * hoop strain (%)
1	Carbon steel	2.0mm thick Stainless steel	6.3	272	0	290	2.6
2	Carbon steel	1.9mm thick Zircaloy -2	5.0	258	0	280	1.5
3	Carbon steel	1.9mm thick Zircaloy -2	7.2	283	0.5	370	3.9
4	Carbon steel	3.4mm thick Stainless steel	5.5	267	0.5	320	1.1
5	Carbon steel	2.0mm thick Stainless steel	5.5	266	1.0	320	1.1

*) measured at a starting point of crack extension.

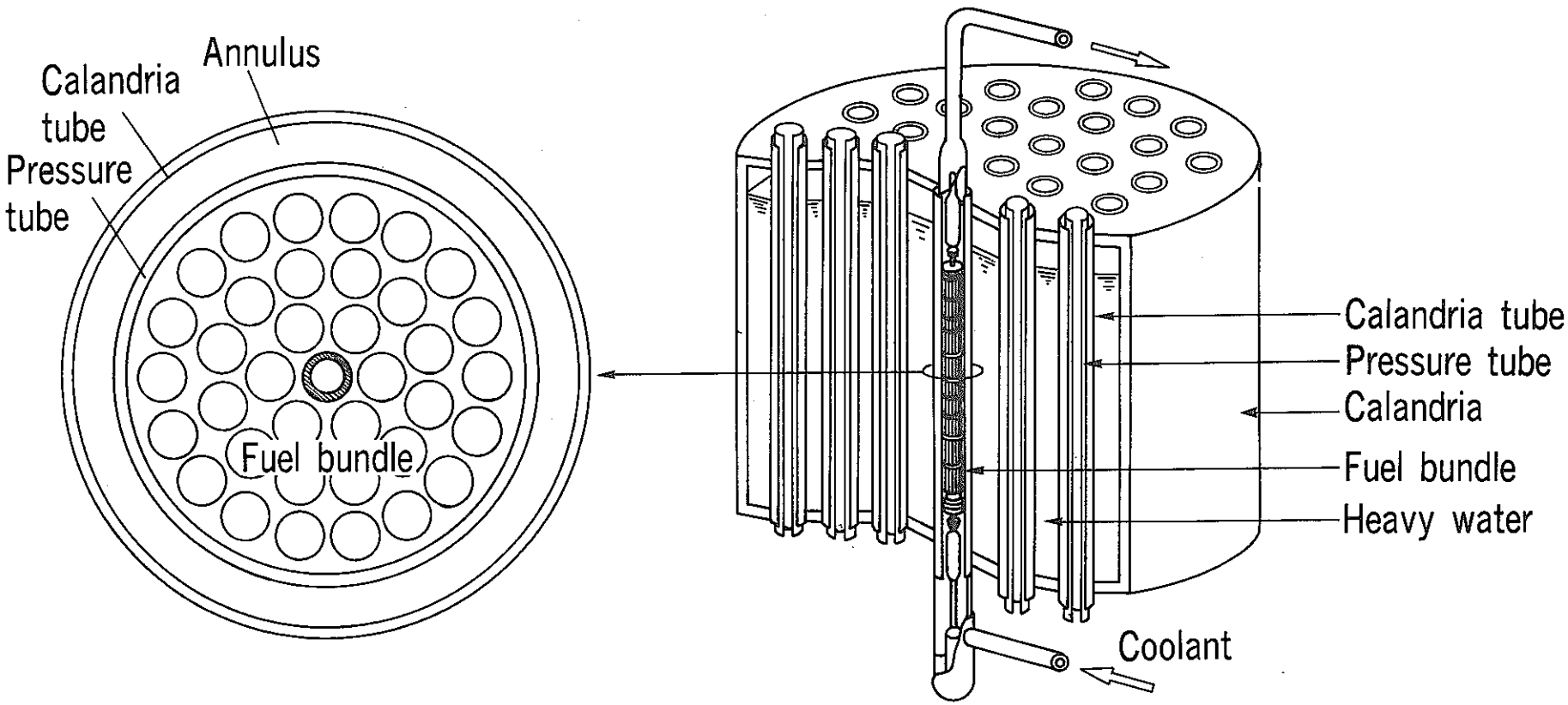

Fig.1 Core of ATR

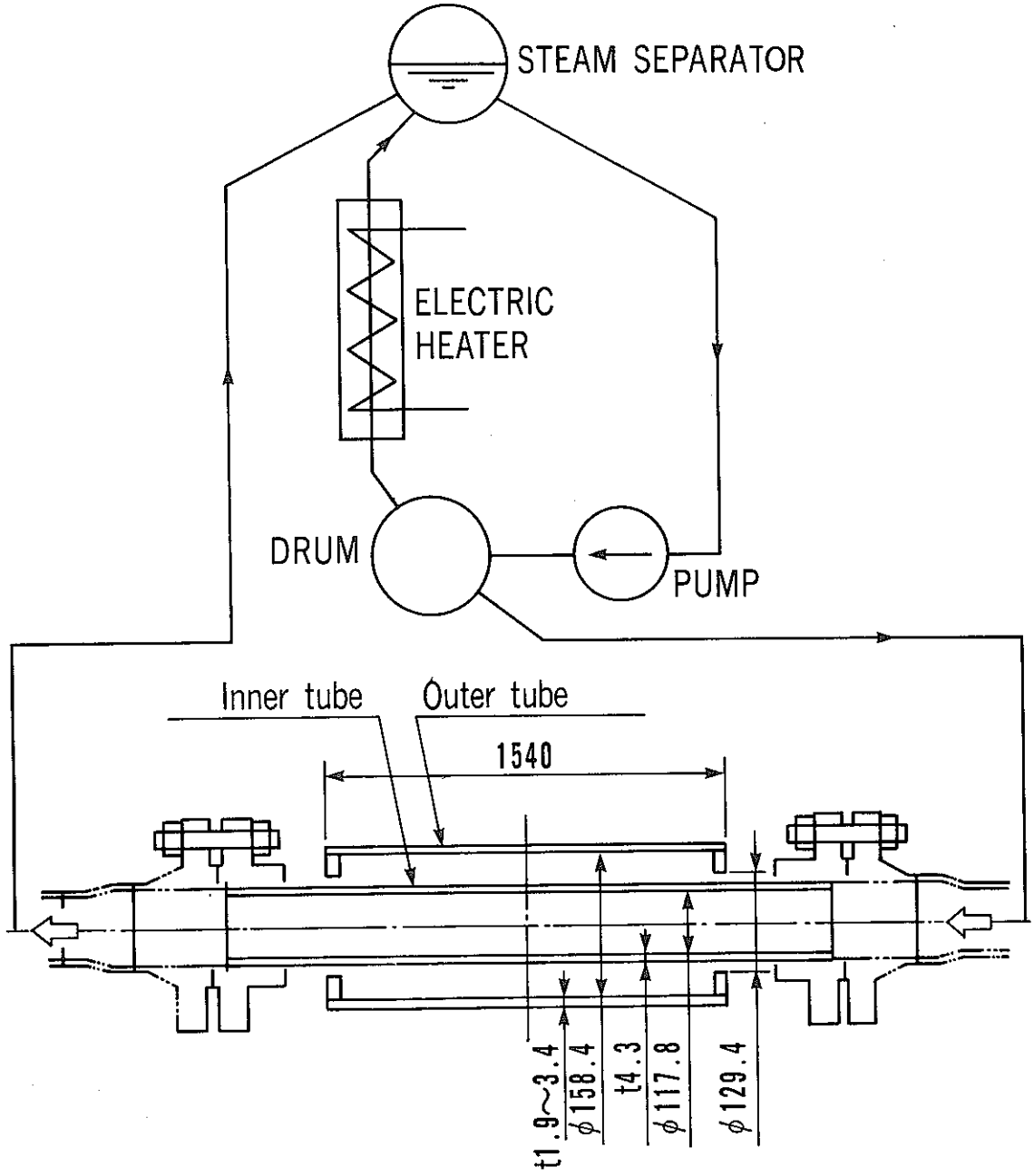

Fig.2 Schematic diagram of test section

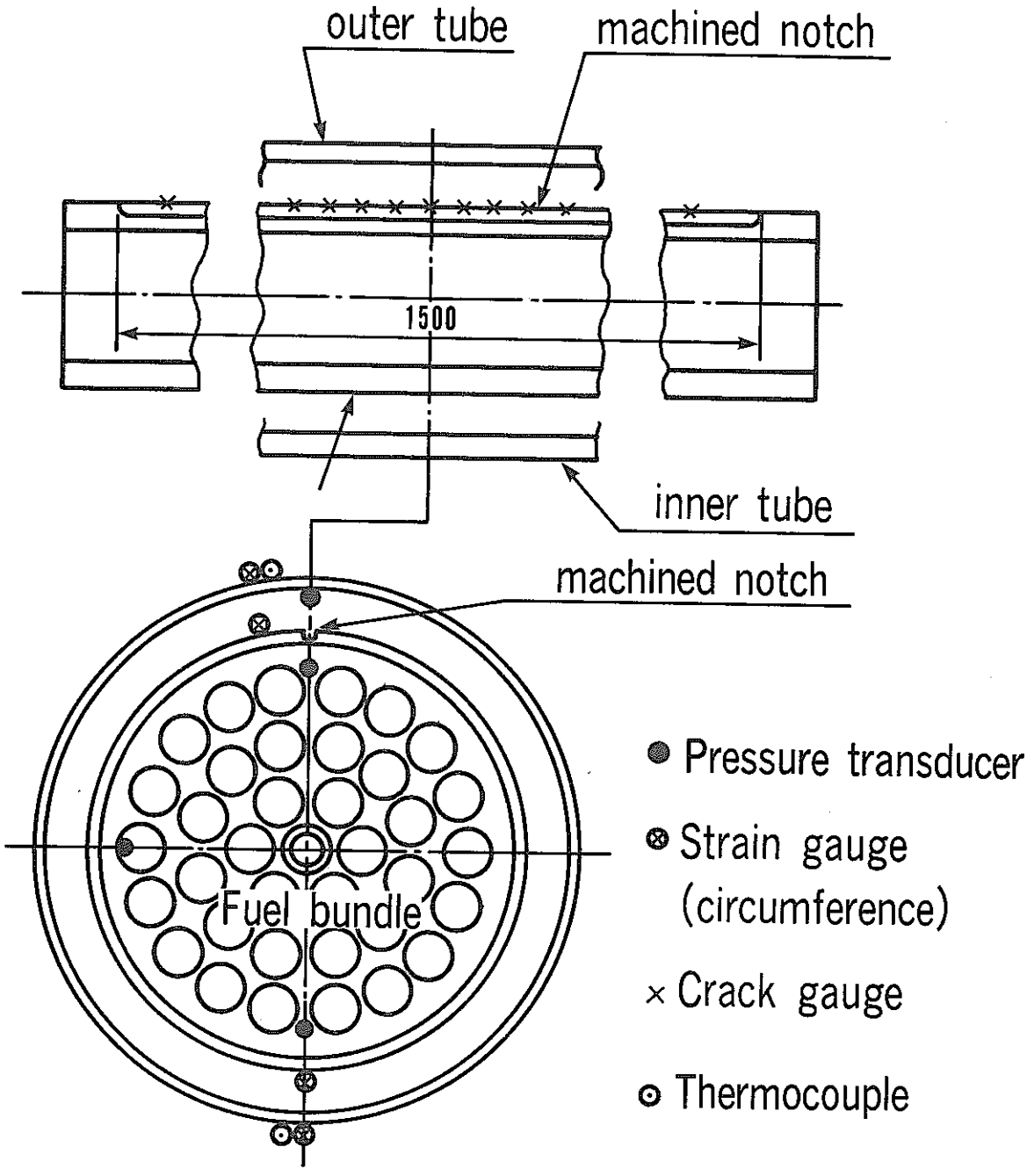

Fig.3 Arrangement of detectors

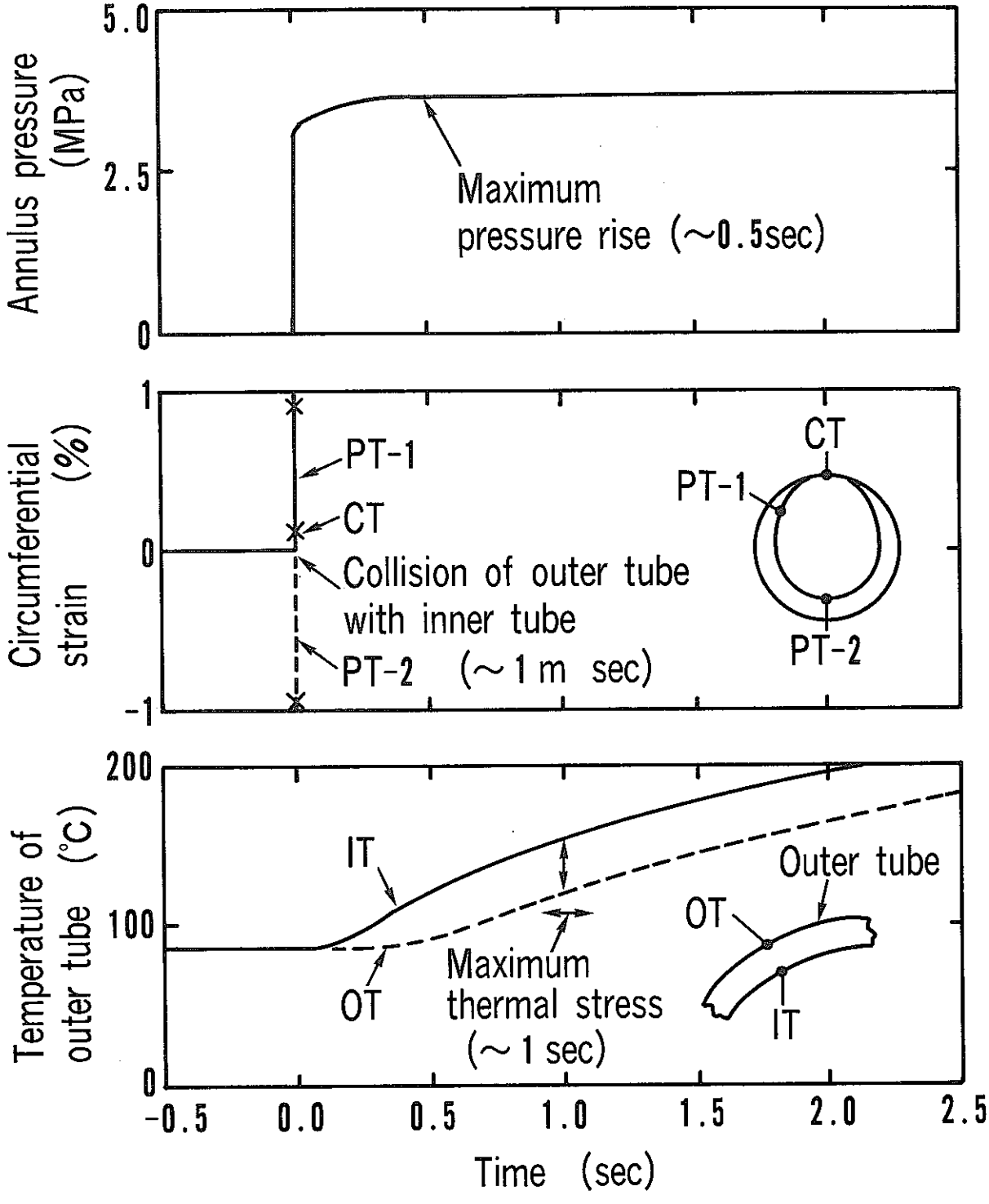

Fig.4 Pressure, strain and temperature histories in experiment
(0sec : initiative time of rupture)

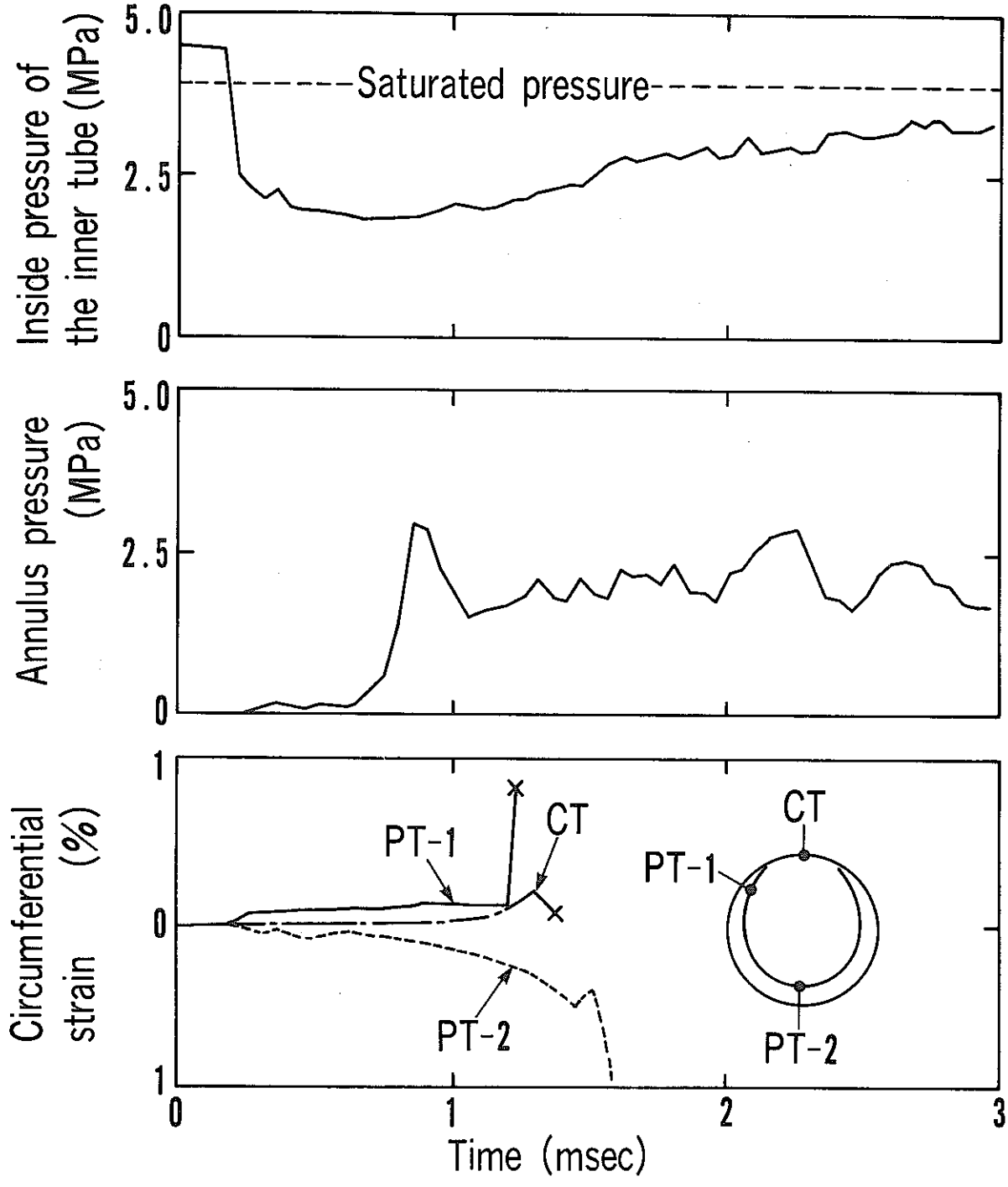

Fig.5 Pressure and strain histories in experiment

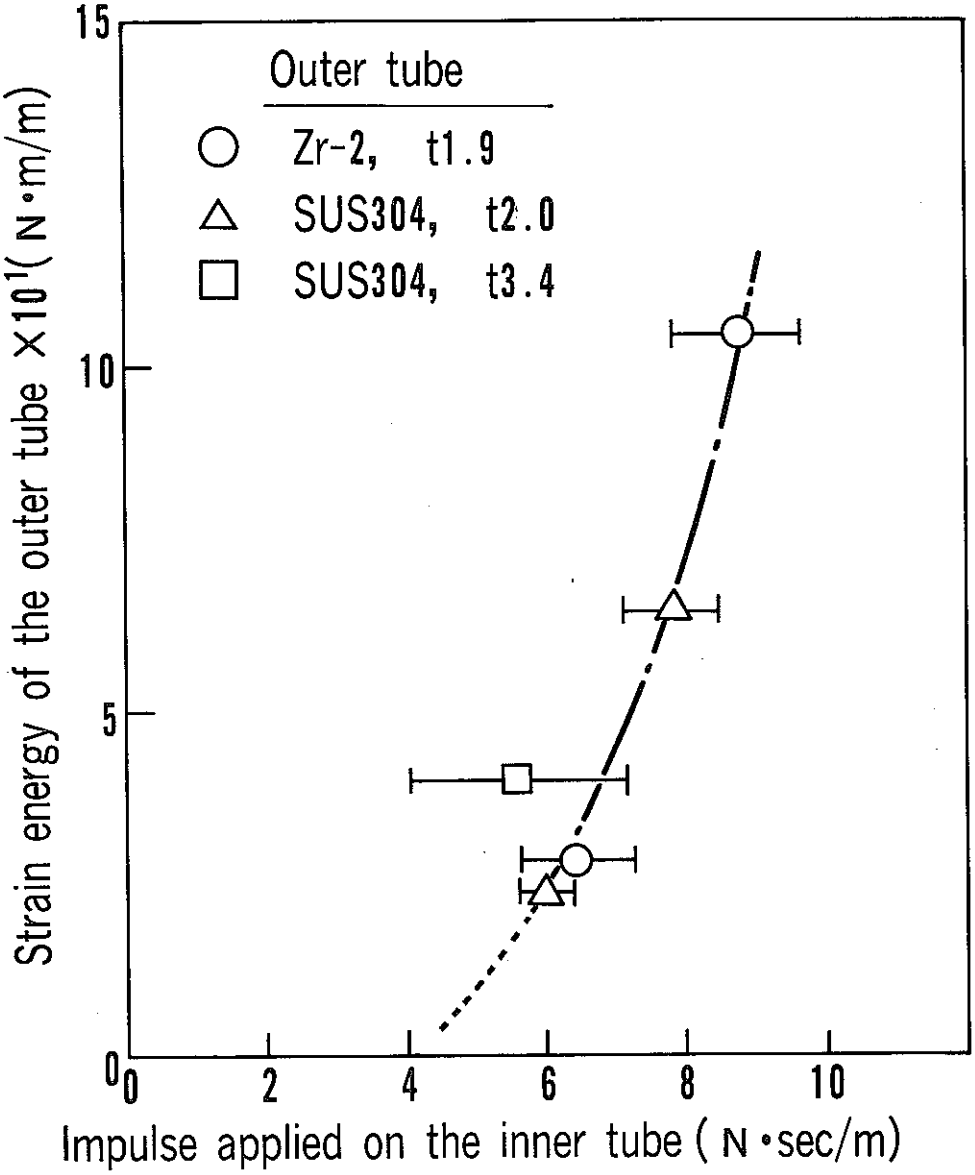

Fig.6 Relation between the impulse applied on the inner tube and the strain energy of the outer tube

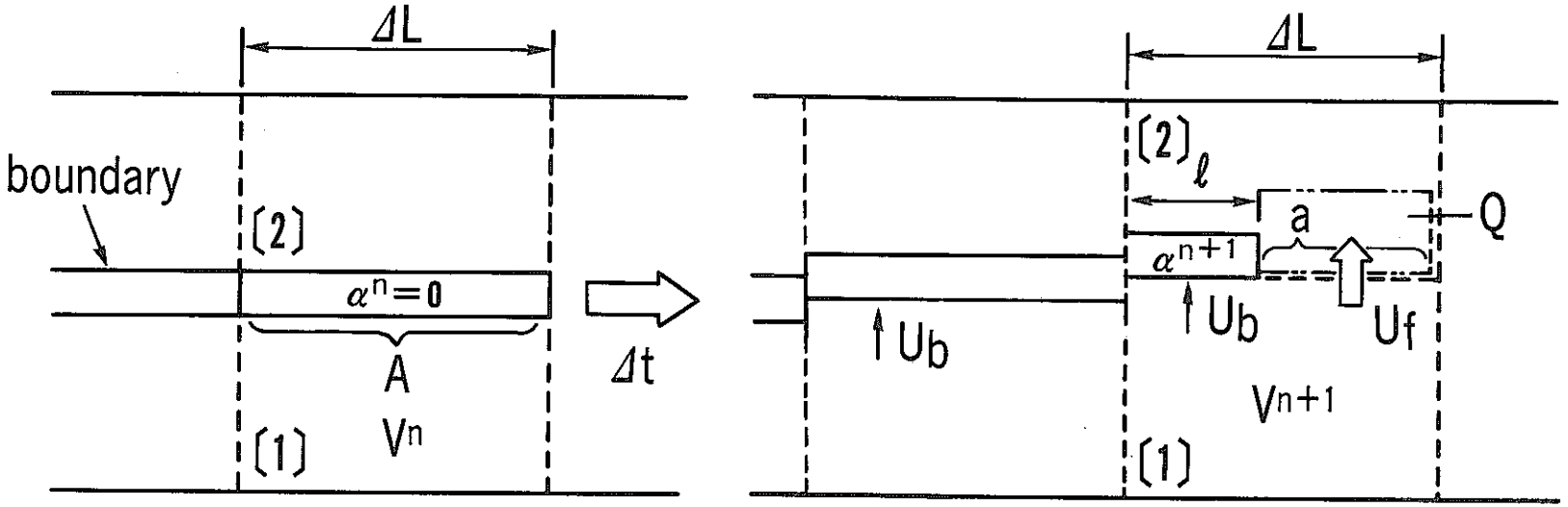

U_f : velocity of fluid

U_b : velocity of boundary

α : transmission factor of boundary

Fig.7 Moving boundary and Porosity model

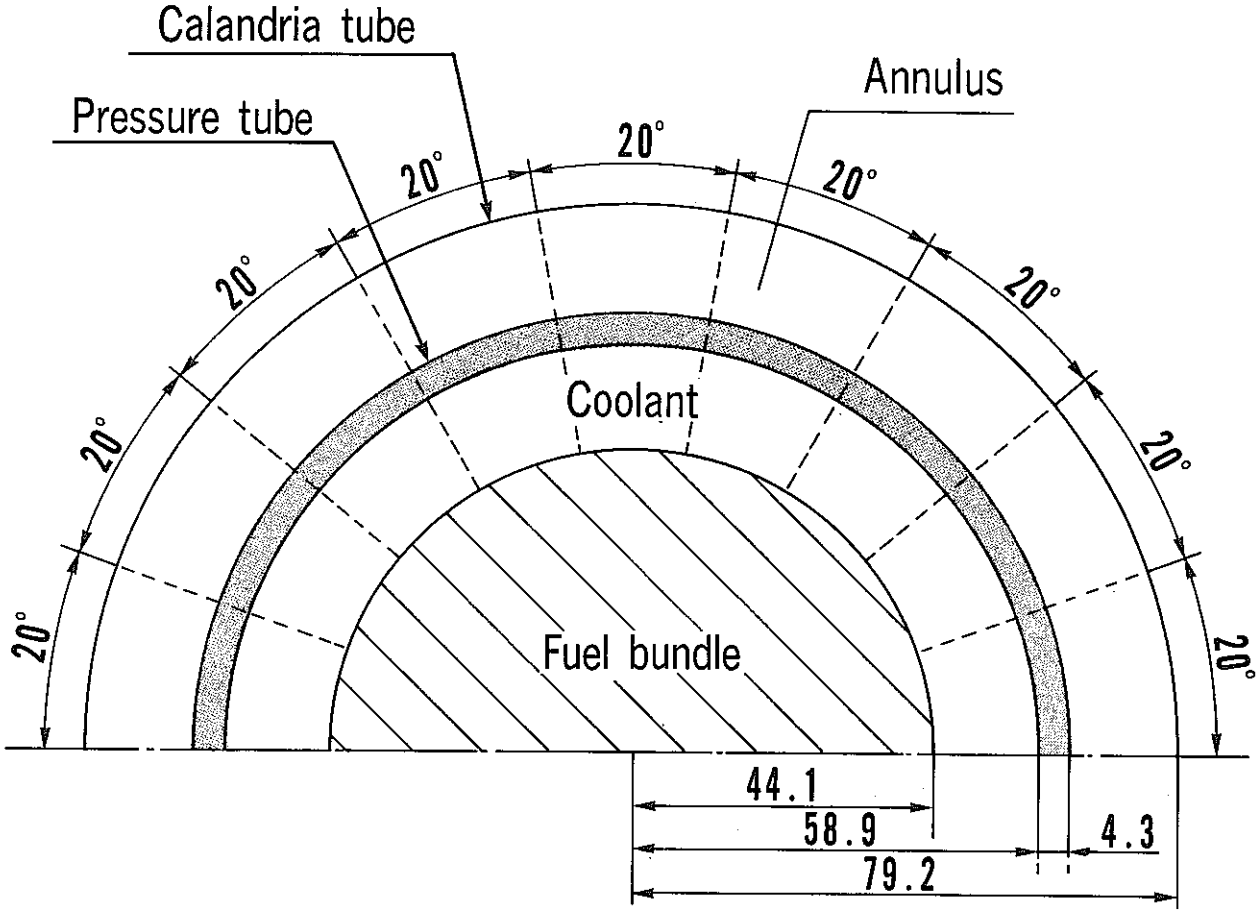

Fig.8 Analytical model for thermal hydraulic analysis

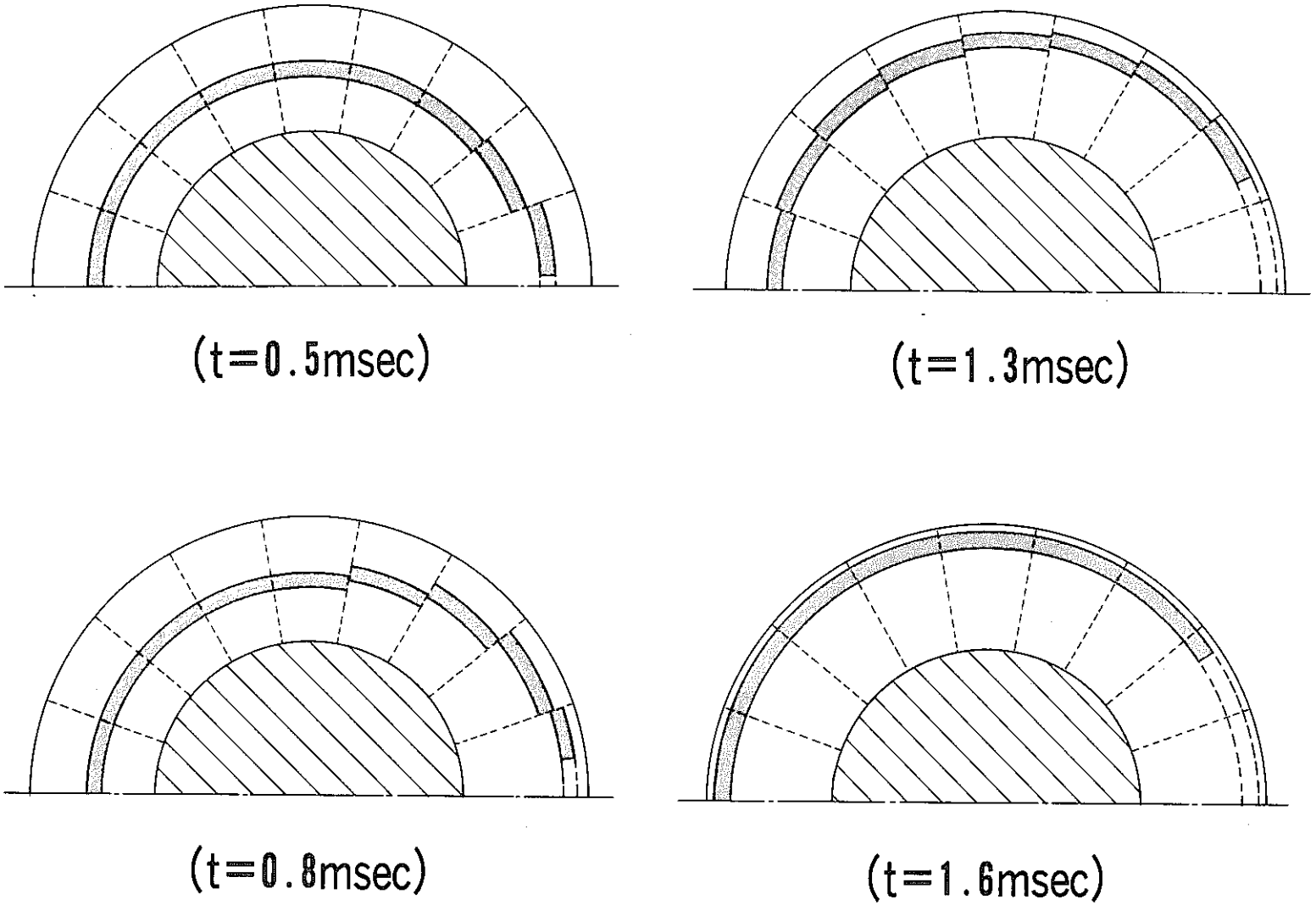

Fig.9 Moving of boundary in experimental analysis

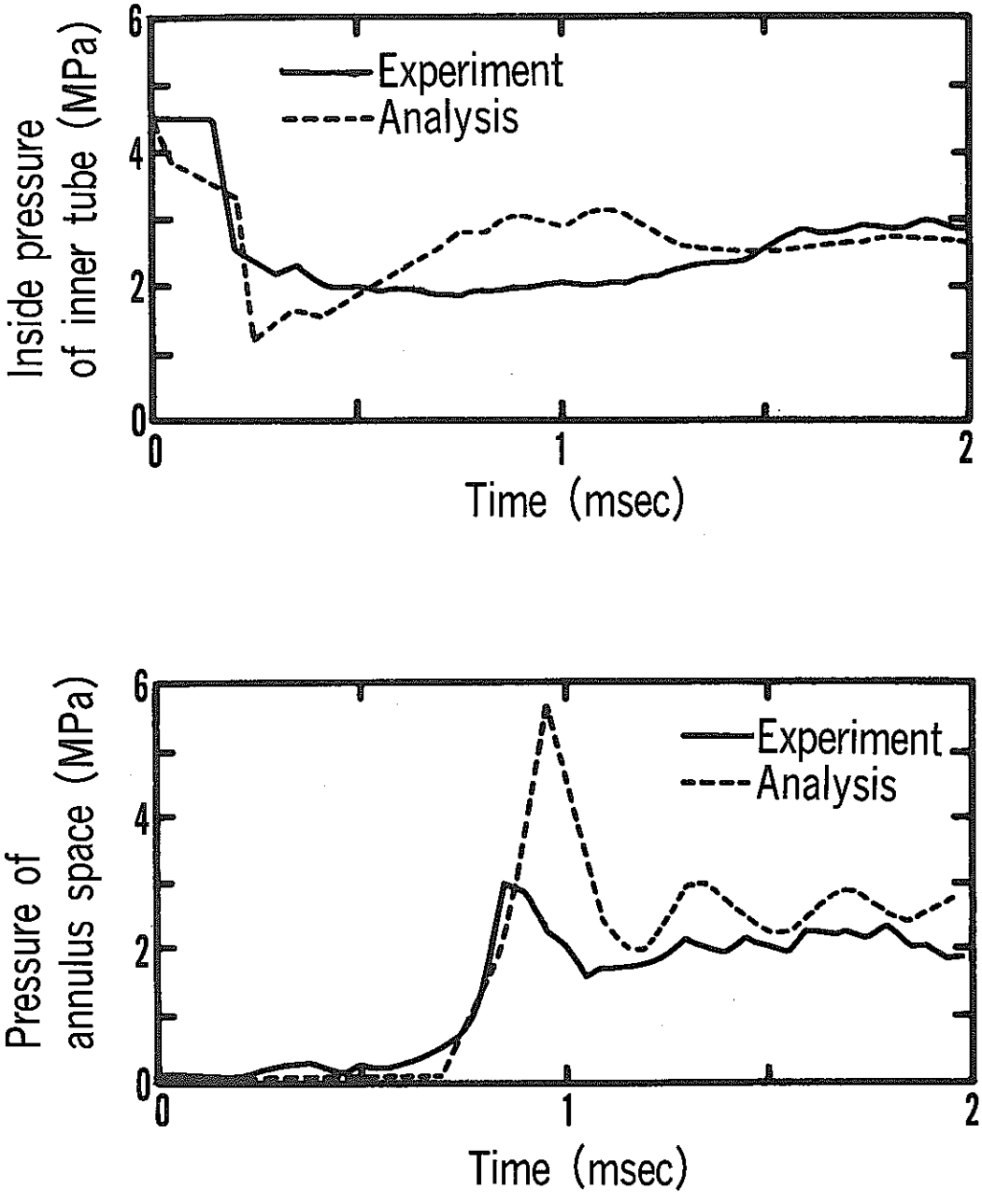

Fig.10 Comparison of calculated results with experimental results

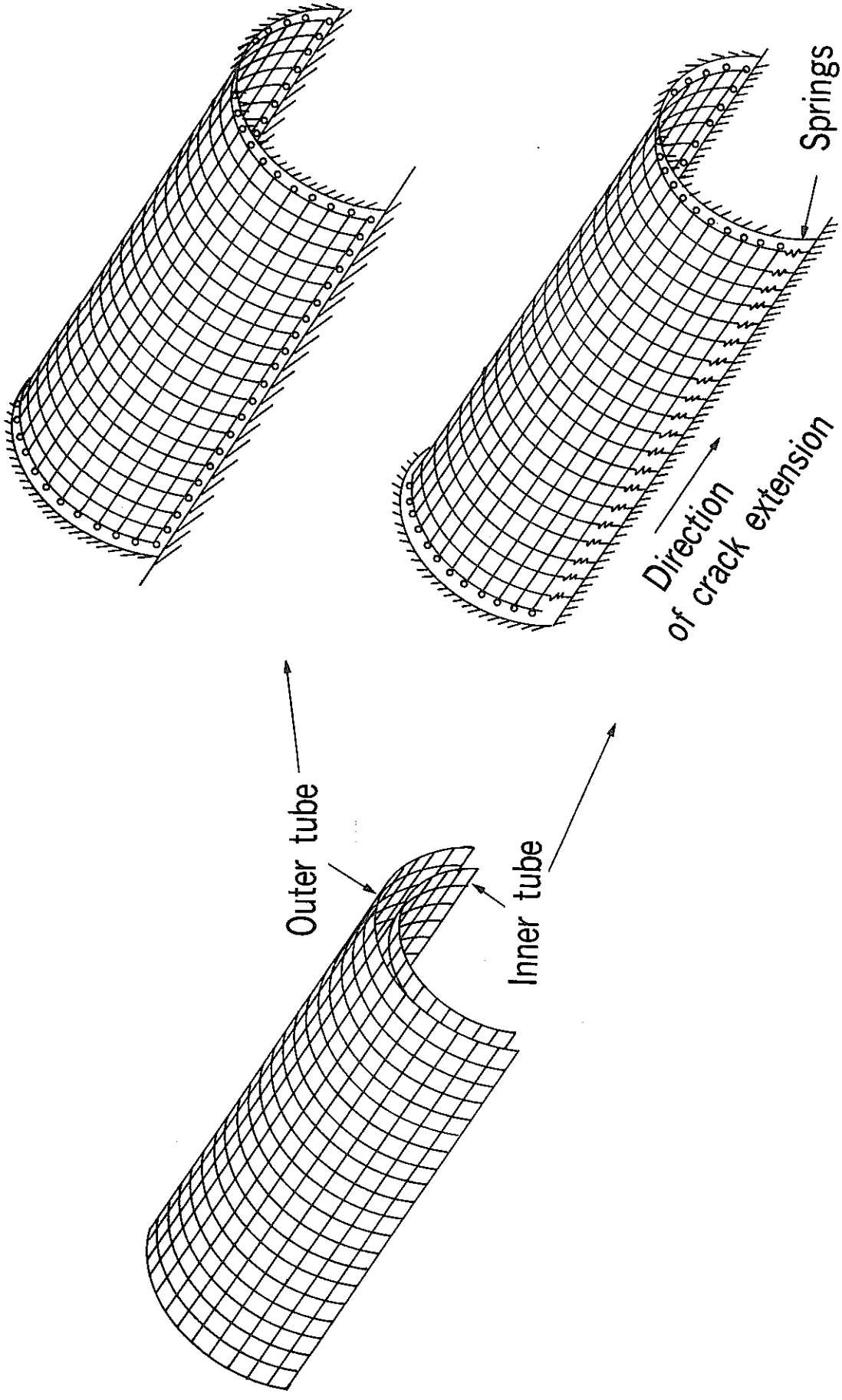

Fig.11 Analytical model for structural analysis

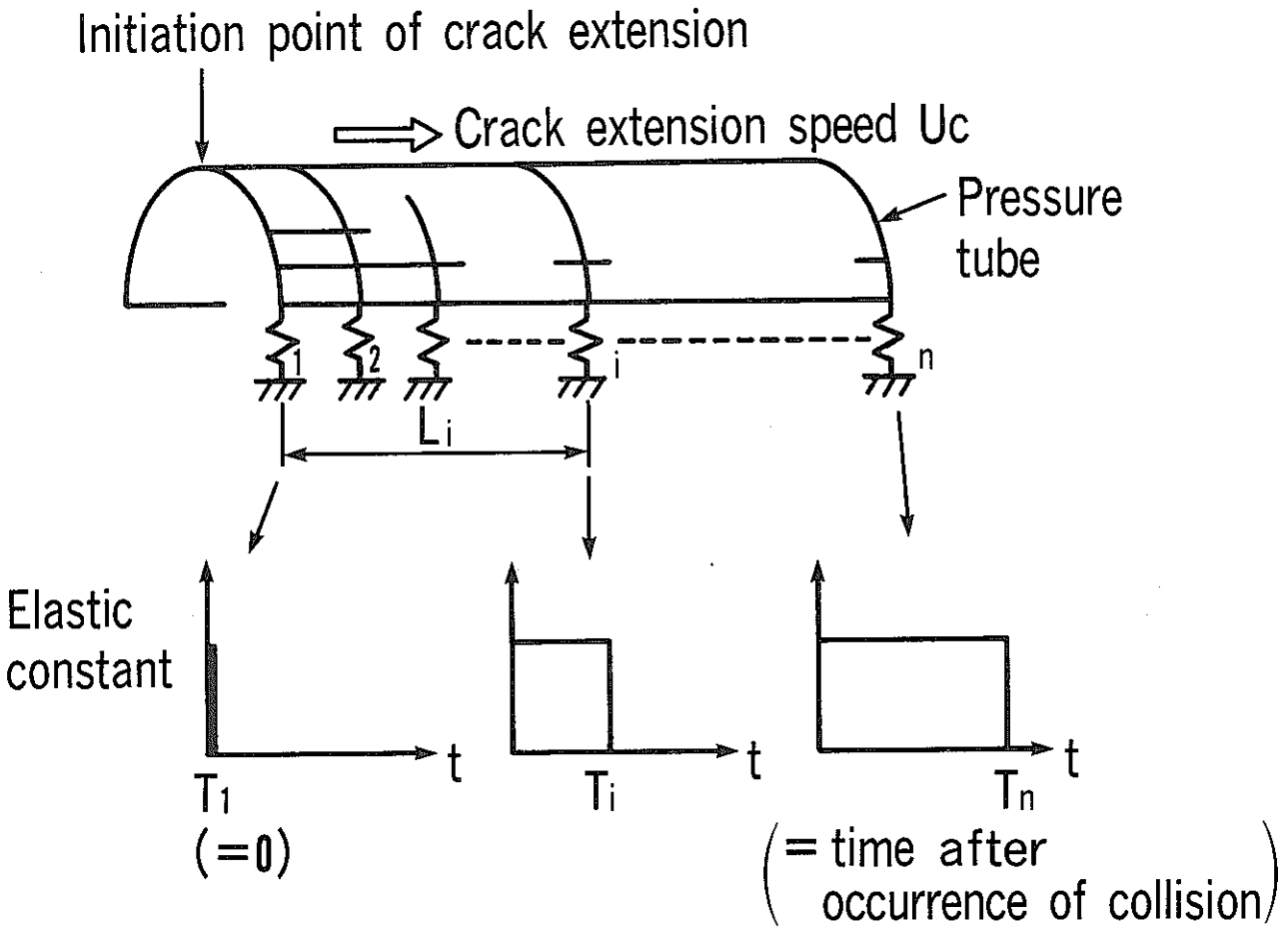

Fig.12 Analytical model for structural analysis and treatment of crack extension

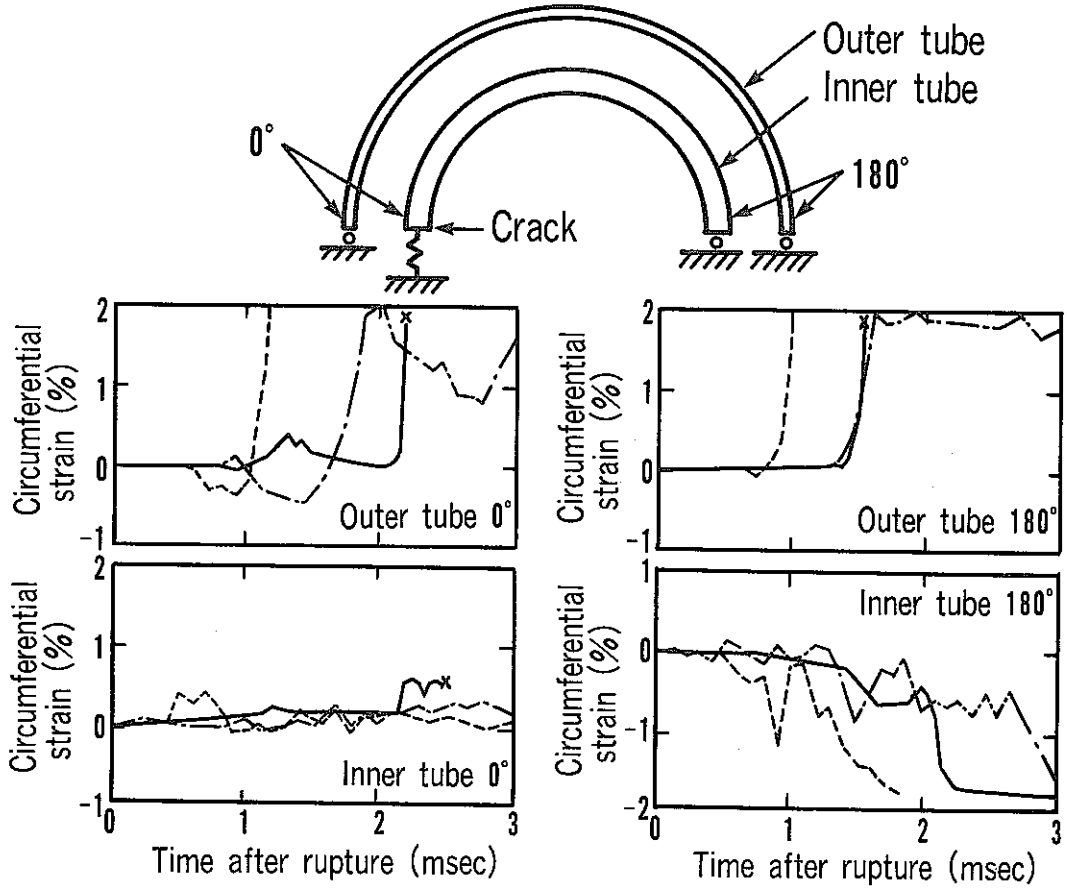

Mean hoop strain (%)		
Experiment	Three dimensional model	Two dimensional model
1.5	1.47	2.49

Experiment
Three dimensional model
Two dimensional model

Fig.13 Comparison of analytical results with experimental results at initiation point of crack extension